photonics

MDPI

Article

Polarization Strips in the Focus of a Generalized Poincaré Beam

Victor V. Kotlyar [1,2], Alexey A. Kovalev [1,2], Alexey M. Telegin [2] and Elena Sergeevna Kozlova [1,2,*]

[1] Image Processing Systems Institute, NRC Kurchatov Institute, Molodogvardeyskaya 151, 443001 Samara, Russia; kotlyar@ipsiras.ru (V.V.K.); alanko@ipsiras.ru (A.A.K.)
[2] Technical Cybernetics Department, Samara National Research University, Moskovskoye Shosse 34, 443086 Samara, Russia; talex85@mail.ru
* Correspondence: kozlova.elena.s@gmail.com

Abstract: We analyze the tight focusing of a generalized Poincaré beam using a Richards–Wolf formalism. Conventional Poincaré beams are superpositions of two Laguerre–Gaussian beams with orthogonal polarization, while the generalized Poincaré beams are composed of two arbitrary optical vortices with rotationally symmetric amplitudes. Analytical relationships for projections of the electric field in the focal plane are derived. Using the superposition of a right-handed circularly polarized plane wave and an optical vortex with a topological charge of −1 as an example, relationships for the intensity distribution and the longitudinal projection of the spin angular momentum vector are deduced. It is theoretically and numerically shown that the original beam has a topological charge of –1/2 and a C-point of circular polarization, and it is generated at the focal plane center, producing an on-axis C-line with a singularity index of –1/2 (a star). Furthermore, when making a full circle of some radius around the optical axis, the major axis vector of polarization ellipse is theoretically and numerically shown to form a one-sided polarization (Möbius) strip of order −3/2, which has three half-twists and a single 'patching' in which two oppositely directed vectors of the major axis of polarization ellipse occur close to each other.

Keywords: polarization Möbius strip; generalized Poincaré beam; tight focusing of light; Richards–Wolf formulae; spin angular momentum; polarization singularity index

Citation: Kotlyar, V.V.; Kovalev, A.A.; Telegin, A.M.; Kozlova, E.S. Polarization Strips in the Focus of a Generalized Poincaré Beam. *Photonics* **2024**, *11*, 430. https://doi.org/10.3390/photonics11050430

Received: 1 February 2024
Revised: 26 April 2024
Accepted: 2 May 2024
Published: 4 May 2024

1. Introduction

On-axis superposition of a left-handed circularly polarized Gaussian beam and a right-handed circularly polarized Laguerre–Gaussian beam with azimuthal number 1 and radial number 0 has been theoretically shown to produce polarization Möbius strips [1]. In this case, a C-line is generated on the superposition of the optical axis. If the LG beam has a minor tilt with respect to the optical axis, when making a circle around the C-point (of circular polarization), the vector of the major axis of polarization ellipse forms a Möbius strip with the number of half-twists increasing with the increasing radius of the circle. A polarization Möbius strip has been experimentally observed [2] at the tight focus of the superposition described in Ref. [1]. It was shown that, for an LG beam with the azimuthal number –1, a polarization Möbius strip formed at the focus around the central C-point with the vector of the major axis of polarization ellipse making three half-twists thanks to the C-point polarization singularity index being –3/2. In addition to the two seminal works we mentioned above, there have been many similar works concerned with polarization Möbius strips. For instance, polarization Möbius strips have been revealed to form in paraxial laser vector beams [3–6]. In particular, it has been shown [6] that when making a circle around a C-point with an integer polarization index, the vector of major/minor axis of polarization ellipse forms a two-sided twisted ribbon with an even number of half-twists. Polarization Möbius strips generated in converging vector beams have also been

described [7–11]. At the focal plane of a linearly polarized Gaussian beam, circularly polarized C-points have been found to occur not on but off the optical axis [7]. It has been numerically and experimentally shown that the vector of the major axis of polarization ellipse forms a single half-twist Möbius strip (with the singularity index of +1/2 or –1/2). Approaches for generating exotic Möbius strips at the focus have been numerically simulated [8]. Polarization Möbius strips at the focus of linearly polarized trigonometric beams have been discussed [11] and shown to also have off-axis C-points around which a Möbius strip is generated by the polarization vector.

It should be noted that, in the above-mentioned works, neither analytical relationships to describe components of the electric field at the focus nor a theoretical explanation of why the polarization Möbius strip was generated at the focus were described. In this work, based on a Richards–Wolf formalism [12], we derive analytical relationships that can be looked upon as an explanation of the experiment described in Ref. [2].

2. Generalized Poincaré Beams at the Tight Focus

A source field in the form of a generalized Poincaré beam [2,13] is described by the Jones vector given by the following:

$$\mathbf{E}(\theta,\varphi) = \alpha A(\theta) e^{in\varphi} \begin{pmatrix} 1 \\ i \end{pmatrix} + \beta A(\theta) e^{im\varphi} \begin{pmatrix} 1 \\ -i \end{pmatrix}, \tag{1}$$

where α and β are complex constants, $A(\theta)$ is the radially symmetric amplitude of the two optical vortices (e.g., a Gauss function), θ is the angle between the optical axis and a straight line connecting a point on the original spherical wavefront with the focal plane center, n and m are topological charges of the right- and left-handed circularly polarized optical vortices, respectively, and φ is the azimuthal angle at the beam cross-section.

The Poincaré beams are coaxial superpositions of two Laguerre–Gaussian beams with different topological charges and with orthogonal polarization states [2,13]. In the current work, by the generalized Poincaré beams (1), we describe a coaxial superposition of two orthogonally polarized optical vortices with different topological charges and with a rotationally symmetric amplitude that can be described by an arbitrary real-valued function $A(\theta)$ depending on the radial coordinate $r = f \cos\theta$.

Using formulae from [14], projections of the electric field in the focal plane can be written as follows:

$$\begin{aligned} E_x &= \alpha i^{n-1} e^{in\varphi} \left(I_{0,n} + e^{i2\varphi} I_{2,n+2} \right) + \beta i^{m-1} e^{im\varphi} \left(I_{0,m} + e^{-i2\varphi} I_{2,m-2} \right), \\ E_y &= \alpha i^{n} e^{in\varphi} \left(I_{0,n} - e^{i2\varphi} I_{2,n+2} \right) + \beta i^{m} e^{im\varphi} \left(-I_{0,m} + e^{-i2\varphi} I_{2,m-2} \right), \\ E_z &= -2\alpha i^{n} e^{i(n+1)\varphi} I_{1,n+1} + 2\beta i^{m} e^{i(m-1)\varphi} I_{1,m-1}. \end{aligned} \tag{2}$$

Equation (2) contains functions $I_{\mu,\nu}$ that depend on the radial variable r and the longitudinal coordinate z:

$$I_{\nu,\mu} = 2kf \int_0^{\alpha} \sin^{\nu+1}\left(\frac{\theta}{2}\right) \cos^{3-\nu}\left(\frac{\theta}{2}\right) \cos^{1/2}(\theta) A(\theta) e^{ikz\cos\theta} J_{\mu}(kr\sin\theta)\, d\theta, \tag{3}$$

where $k = 2\pi/\lambda$ is the wave number of light of wavelength λ, f is the focal length of a focusing lens, α is the maximum angle of the ray tilt to the optical axis, which defines the aplanatic lens NA: NA = sin α, and $J_\nu(\xi)$ is the Bessel function of the ν-th order and first kind.

As was the case in Refs. [1,2], in superposition (1), we put $n = 0$, $m = -1$, and $\alpha = \beta = 1$. Then, Equation (1) is rearranged to the following:

$$\mathbf{E}(\theta,\varphi) = A(\theta)\begin{pmatrix}1\\ i\end{pmatrix} + A(\theta)e^{-i\varphi}\begin{pmatrix}1\\ -i\end{pmatrix} = 2A(\theta)e^{-i\varphi/2}\begin{pmatrix}\cos\left(\frac{\varphi}{2}\right)\\ -\sin\left(\frac{\varphi}{2}\right)\end{pmatrix}. \quad (4)$$

From (4), the topological charge of the original beam is seen to equal –1/2, with the polarization singularity of field (4) also being equal to –1/2. Actually, in the cross-section of field (4), linear polarization is inhomogeneous and has a polarization singularity line at $\varphi = 0$, which is a line (horizontal semi-axis) where polarization is indefinite, as at angles slightly larger than $\varphi = 0$, polarization is horizontally directed to the right, whereas at angles slightly less than 2π, polarization is horizontally directed to the left. After making a full circle centered on the beam center, the linear polarization vector rotates clockwise by π, meaning that for field (4), the polarization singularity index is I = –1/2. In the meantime, as field (4) propagates, a C-point of circular polarization is formed at the center.

For field (4), instead of Equation (2), the electric field projections in the plane of tight focus reads as follows:

$$\begin{aligned} E_x &= -i\left(I_{0,0} + e^{i2\varphi}I_{2,2}\right) + e^{-i\varphi}\left(I_{0,1} + e^{-i2\varphi}I_{2,3}\right),\\ E_y &= \left(I_{0,0} - e^{i2\varphi}I_{2,2}\right) - ie^{-i\varphi}\left(I_{0,1} - e^{-i2\varphi}I_{2,3}\right),\\ E_z &= -2e^{i\varphi}I_{1,1} - 2ie^{-i2\varphi}I_{1,2}. \end{aligned} \quad (5)$$

From (5), the on-axis electric field projections ($r = 0$) are seen to take the form:

$$\begin{pmatrix}E_x(r\to 0)\\ E_x(r\to 0)\end{pmatrix} \approx \begin{pmatrix}-iI_{0,0} + e^{-i\varphi}I_{0,1}\\ I_{0,0} - ie^{-i\varphi}I_{0,1}\end{pmatrix} = -iI_{0,0}\begin{pmatrix}1\\ i\end{pmatrix} + e^{-i\varphi}I_{0,1}\begin{pmatrix}1\\ -i\end{pmatrix}. \quad (6)$$

At the center of the focal plane, there is a C-point of right-handed circular polarization. As seen from Equation (6), the polarization singularity index near the C-point equals I = –1/2 (star-type), as for the initial field (4).

From (5), the intensity of the on-axis field projection in the focal plane is as follows:

$$I_z = |E_z|^2 = 4\left(I_{1,1}^2 + I_{1,2}^2 + 2I_{1,1}I_{1,2}\sin 3\varphi\right) \quad (7)$$

With the intensity dependent on the triple azimuthal angle, when making a full circle of some radius around the optical axis, three maxima are found on the circle: at angles $\varphi = \pi/6$, $5\pi/6$, and $3\pi/2$, with the intensity pattern in the form of three intensity spots centered on the maxima. Relationships to describe transverse intensity projections are more complex:

$$\begin{aligned} I_x &= |E_x|^2 = \left(I_{0,0}^2 + I_{2,2}^2 + I_{0,1}^2 + I_{2,3}^2\right) + 2I_{0,0}I_{0,1}\sin\varphi + 2\cos 2\varphi\left(I_{0,0}I_{2,2} + \right.\\ &\left. + I_{0,1}I_{2,3}\right) + 2\sin 3\varphi\left(I_{0,0}I_{2,3} + I_{0,1}I_{2,2}\right) + 2I_{2,2}I_{2,3}\sin 5\varphi,\\ I_y &= |E_y|^2 = \left(I_{0,0}^2 + I_{2,2}^2 + I_{0,1}^2 + I_{2,3}^2\right) - 2I_{0,0}I_{0,1}\sin\varphi - 2\cos 2\varphi\left(I_{0,0}I_{2,2} + \right.\\ &\left. + I_{0,1}I_{2,3}\right) + 2\sin 3\varphi\left(I_{0,0}I_{2,3} + I_{0,1}I_{2,2}\right) - 2I_{2,2}I_{2,3}\sin 5\varphi. \end{aligned} \quad (8)$$

It has been shown [15] that a major contribution to the field energy comes from the $I_{\nu,\mu}$ component with zero first index ($I_{0,\mu}$). With the contribution from the components $I_{1,\mu}$ being essentially less and from $I_{2,\mu}$ being even lesser, in (8), we retain only terms containing $I_{0,\mu}$. Thus, relationships depicted in (8) are approximately given by the following:

$$\begin{aligned} I_x &\approx I_{0,0}^2 + I_{0,1}^2 + 2I_{0,0}I_{0,1}\sin\varphi,\\ I_y &\approx I_{0,0}^2 + I_{0,1}^2 - 2I_{0,0}I_{0,1}\sin\varphi. \end{aligned} \quad (9)$$

From (9), the intensity I_x is seen to have a single maximum lying on the vertical axis in the upper semi-plane with the intensity I_y also having a single maximum lying on the vertical axis but in the lower semi-plane. Such an intensity pattern is in agreement with that derived experimentally [2].

Next, we find the longitudinal projection of the spin angular momentum (SAM) vector, $\mathbf{S} = \mathrm{Im}\left(\mathbf{E}^* \times \mathbf{E}\right)$, in the focal plane for original field (4):

$$S_z = 2\left(I_{0,0}^2 + I_{2,3}^2 - I_{0,1}^2 - I_{2,2}^2\right) + 4\sin 3\varphi\left(I_{0,0}I_{2,3} - I_{0,1}I_{2,2}\right). \tag{10}$$

The longitudinal SAM component distribution in (10) is seen to be similar to the longitudinal intensity distribution in (7), as both relationships contain the sine function of the triple azimuthal angle. Hence, similar to the intensity in (7), the SAM distribution in (10) has three maxima lying at angles $\varphi = \pi/6$, $5\pi/6$, and $3\pi/2$. Meanwhile, minimal SAM values are found at angles $\varphi = \pi/2$, $7\pi/6$, and $-\pi/6$. At points where the longitudinal SAM component has a near-zero minimal value, the polarization ellipse is almost perpendicular to the focal plane. Below, we show that it is approximately at those points (or, putting it more exactly, at those angles) where twists of a polarization Möbius strip occur, which is generated by the major/minor axis of the polarization ellipse when moving along a certain circle centered on the on-axis C-point.

3. Polarization Ellipse at the Focus of a Generalized Poincaré Beam

The location of the major/minor axis of the polarization ellipse in the focal plane can be derived using the Berry formulae [16], which enable the polarization singularity index to be calculated for arbitrary vector fields. Following the said formulae, the electric field vector **E** can be expressed via real vectors **A** and **B** that are extended along the major and minor axes of the polarization vector at a given point of space:

$$\begin{aligned}
&\mathbf{E} = e^{i\gamma}(\mathbf{A} + i\mathbf{B}),\ I = |\mathbf{A}|^2 + |\mathbf{B}|^2,\\
&\mathbf{A}\bullet\mathbf{B} = 0,\ |\mathbf{A}| \geq |\mathbf{B}|,\\
&\gamma = \frac{1}{2}\arg\left(\mathbf{E}\bullet\mathbf{E}\right),\\
&\mathbf{A} = \frac{1}{\left|\sqrt{\mathbf{E}\bullet\mathbf{E}}\right|}\mathrm{Re}\left(\mathbf{E}\sqrt{\mathbf{E}^*\bullet\mathbf{E}^*}\right),\\
&\mathbf{B} = \frac{1}{\left|\sqrt{\mathbf{E}\bullet\mathbf{E}}\right|}\mathrm{Im}\left(\mathbf{E}\sqrt{\mathbf{E}^*\bullet\mathbf{E}^*}\right),\\
&\mathbf{S} = \mathrm{Im}\left(\mathbf{E}^* \times \mathbf{E}\right) = 2(\mathbf{A}\times\mathbf{B}).
\end{aligned} \tag{11}$$

In Equation (11), $\bullet$ denotes a dot product of vectors, $\times$ is a cross product, Re and Im are the real and imaginary parts of the number, **S** simultaneously defines the SAM vector and the normal vector to the polarization ellipse plane formed by the vectors **A** and **B**, and I is the intensity expressed via projections of the vectors of the polarization ellipse axes. Separating in field (5) the real and imaginary parts, projections of the vectors **A** and **B** are given by the following:

$$
\begin{aligned}
&\mathbf{E} = e^{-i3\varphi/2}(\mathbf{A} + i\mathbf{B}),\\
&A_x = I_{0,0}\sin\left(\frac{3\varphi}{2}\right) + I_{2,2}\sin\left(\frac{7\varphi}{2}\right) + I_{0,1}\cos\left(\frac{\varphi}{2}\right) + I_{2,3}\cos\left(\frac{3\varphi}{2}\right),\\
&A_y = I_{0,0}\cos\left(\frac{3\varphi}{2}\right) - I_{2,2}\cos\left(\frac{7\varphi}{2}\right) + I_{0,1}\sin\left(\frac{\varphi}{2}\right) + I_{2,3}\sin\left(\frac{3\varphi}{2}\right),\\
&A_z = -2I_{1,1}\cos\left(\frac{5\varphi}{2}\right) - 2I_{1,2}\sin\left(\frac{\varphi}{2}\right),\\
&B_x = -I_{0,0}\cos\left(\frac{3\varphi}{2}\right) - I_{2,2}\cos\left(\frac{7\varphi}{2}\right) + I_{0,1}\sin\left(\frac{\varphi}{2}\right) - I_{2,3}\sin\left(\frac{3\varphi}{2}\right),\\
&B_y = I_{0,0}\sin\left(\frac{3\varphi}{2}\right) - I_{2,2}\sin\left(\frac{7\varphi}{2}\right) - I_{0,1}\cos\left(\frac{\varphi}{2}\right) + I_{2,3}\cos\left(\frac{3\varphi}{2}\right),\\
&B_z = -2I_{1,1}\sin\left(\frac{5\varphi}{2}\right) - 2I_{1,2}\cos\left(\frac{\varphi}{2}\right).
\end{aligned}
\tag{12}
$$

The vectors in Equation (12) lie on the polarization ellipse but are not mutually orthogonal. However, by taking into account just the highest contributing terms, the vectors **A** and **B** in (12) can be considered approximately orthogonal and expressed as follows:

$$
\begin{aligned}
&A_x \approx I_{0,0}\sin\left(\frac{3\varphi}{2}\right) + I_{0,1}\cos\left(\frac{\varphi}{2}\right),\\
&A_y \approx I_{0,0}\cos\left(\frac{3\varphi}{2}\right) + I_{0,1}\sin\left(\frac{\varphi}{2}\right),\\
&A_z = -2I_{1,1}\cos\left(\frac{5\varphi}{2}\right) - 2I_{1,2}\sin\left(\frac{\varphi}{2}\right) \approx 0,\\
&B_x \approx -I_{0,0}\cos\left(\frac{3\varphi}{2}\right) + I_{0,1}\sin\left(\frac{\varphi}{2}\right),\\
&B_y \approx I_{0,0}\sin\left(\frac{3\varphi}{2}\right) - I_{0,1}\cos\left(\frac{\varphi}{2}\right),\\
&B_z = -2I_{1,1}\sin\left(\frac{5\varphi}{2}\right) - 2I_{1,2}\cos\left(\frac{\varphi}{2}\right) \approx 0.
\end{aligned}
\tag{13}
$$

Near the optical axis, the second terms are negligibly small compared to the first ones and can be dropped; thus, the components of the vector **A** can be read as follows:

$$
\begin{aligned}
&A_x(kr \ll 1) \approx I_{0,0}\sin\left(\frac{3\varphi}{2}\right),\\
&A_y(kr \ll 1) \approx I_{0,0}\cos\left(\frac{3\varphi}{2}\right),\\
&A_z(kr \ll 1) \approx 0.
\end{aligned}
\tag{14}
$$

Expressions depicted in (14) are easy to analyze. We have already shown that a C-point with index I = –1/2 is generated near the optical axis. From (14), one can infer that, at some distance from the focal spot center, the tip of the vector **A** makes not one but three half-twists by angle π. Hence, at a distance from the center, the polarization singularity index of the focal field equals I = –3/2. Actually, the vector **A** is directed vertically upwards at φ = 0, vertically downwards at φ = 2π/3, again vertically upwards at φ = 4π/3, and again vertically downwards at φ = 2π. We note that, in Ref. [2], the polarization singularity index at the focus also had a negative value (I = −1/2). The fact is that the intensity patterns in this work and in Ref. [2] are mutually rotated by π. Thus, Equation (14) suggests that when moving in the focal plane along a circle centered on the optical axis the polarization ellipse' vector **A** generates a one-sided, Möbius strip-type surface with the half-twists occurring at angles φ = π/3, π, and 5π/3, with a 'patch' line (where two oppositely directed

vectors **A** meet) found at $\varphi = 0, 2\pi$. It is worth noting that the Möbius strip described herein is different from that discussed in Ref. [2], being rotated by $\pi/2$. For the Möbius strip, the polarization index is assumed to be positive if moving clockwise on a circle, leading to the Möbius strip twisting clockwise as well. By analogy, the index is negative if moving on a circle anticlockwise (as shown in Figure 1), and the Möbius strip is also twisted anticlockwise.

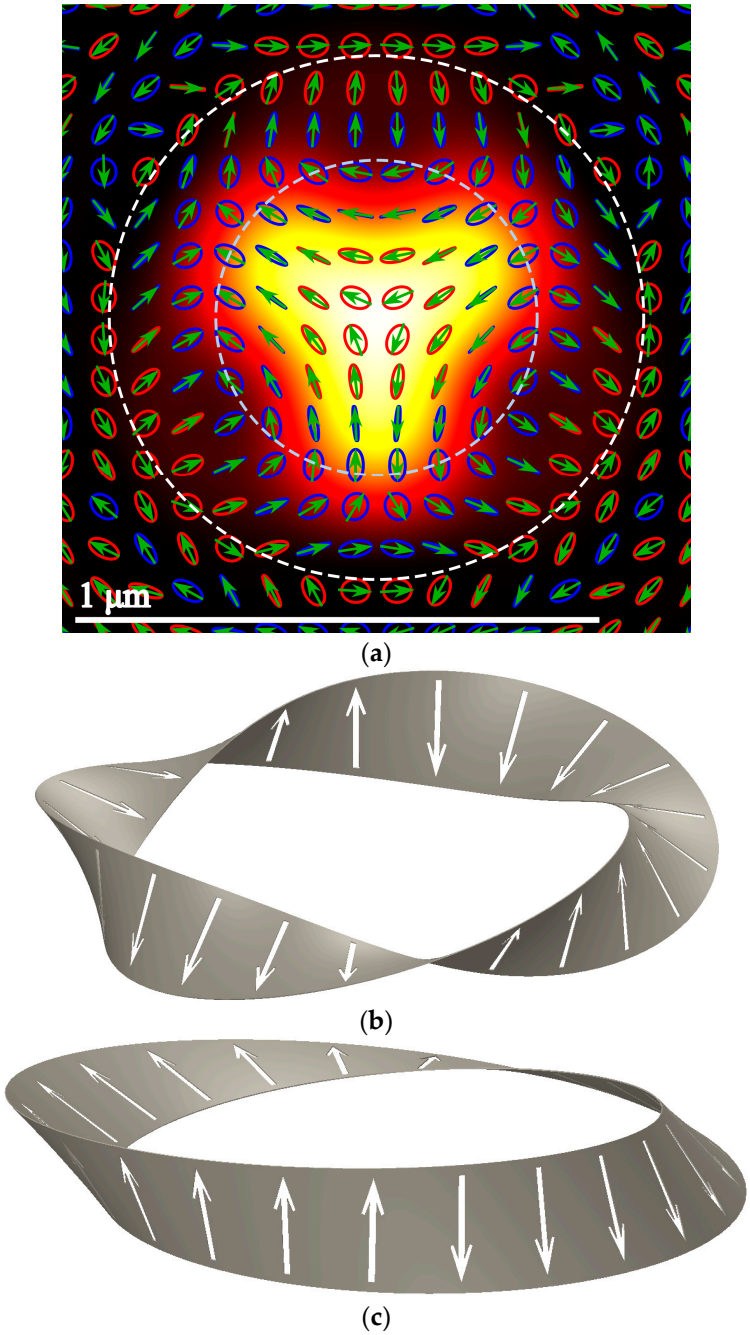

Figure 1. Intensity pattern in the focal plane from the original field (4) forms a colored (yellow-red) triangle with a downward apex (**a**); arrows within the polarization ellipses mark the major axis vectors: red ellipses have a positive projection on the optical axis and blue ones have a negative projection. A white horizontal line in the bottom is 1 μm long. A white dashed circle is where a polarization Möbius strip with three half-twists and index –3/2 is generated. The polarizing Möbius strip has three half-turns and an index of −3/2. It is deposed along the white dotted circle (**b**). The gray dotted circle of smaller radius passes through the polarization ellipses, which make one half turn and one stitch. Therefore, the polarizing Möbius strip on this small circle (**c**) has an index of −1/2.

4. Two-Sided Polarization Strips with an Even Number of Half-Twists

Putting $n = 0$ and $m = -2$ in Equation (1) for the generalized Poincaré beam, the initial field in (4) is replaced by the following:

$$\mathbf{E}(\theta,\varphi) = A(\theta)\begin{pmatrix}1\\ i\end{pmatrix} + A(\theta)e^{-i2\varphi}\begin{pmatrix}1\\ -i\end{pmatrix} = 2A(\theta)e^{-i\varphi}\begin{pmatrix}\cos(\varphi)\\ -\sin(\varphi)\end{pmatrix}. \quad (15)$$

Field (15) has a topological charge of –1, describing an optical vortex with cylindrical polarization, which is a modification of radial polarization with its linear polarization vectors lying along hyperbolas. When making a full circle around the optical axis, the linear polarization vector in Equation (15) makes two half-twists meaning that the polarization singularity index equals I= –1. On the optical axis, there is a V-point polarization singularity where linear polarization is indefinite. Thus, in the focal plane, field (15) has the following projections of the electric field:

$$\begin{aligned} E_x &= -i\left(I_{0,0} + e^{i2\varphi}I_{2,2}\right) + ie^{-i2\varphi}\left(I_{0,2} + e^{-i2\varphi}I_{2,4}\right),\\ E_y &= \left(I_{0,0} - e^{i2\varphi}I_{2,2}\right) + e^{-i2\varphi}\left(I_{0,2} - e^{-i2\varphi}I_{2,4}\right),\\ E_z &= -2e^{i\varphi}I_{1,1} + 2e^{-i3\varphi}I_{1,3}. \end{aligned} \quad (16)$$

Similarly to Equation (6), Equation (16) allows obtaining an expression for transverse components of the field (15) near the optical axis:

$$\begin{pmatrix}E_x(r\to 0)\\ E_x(r\to 0)\end{pmatrix} \approx \begin{pmatrix}-iI_{0,0} + ie^{-2i\varphi}I_{0,2}\\ I_{0,0} + e^{-2i\varphi}I_{0,2}\end{pmatrix} = -iI_{0,0}\begin{pmatrix}1\\ i\end{pmatrix} + ie^{-2i\varphi}I_{0,2}\begin{pmatrix}1\\ -i\end{pmatrix}. \quad (16.1)$$

From (16.1), it can be seen that there is a C-point of right-handed circular polarization with the same polarization singularity index as in the original field: I = –1.

For field (15), the longitudinal spin density in the focal plane reads as follows:

$$S_z = 2\left(I_{0,0}^2 + I_{2,4}^2 - I_{0,2}^2 - I_{2,2}^2\right) + 4\cos 4\varphi\left(I_{0,0}I_{2,4} - I_{0,2}I_{2,2}\right). \quad (17)$$

The longitudinal intensity distribution in the focal plane reads as follows:

$$I_z = |E_z|^2 = 4\left(I_{1,1}^2 + I_{1,3}^2 - 2I_{1,1}I_{1,2}\cos 4\varphi\right). \quad (18)$$

Unlike Equations (7) and (10), it is seen from (17) and (18) that the patterns of intensity and longitudinal spin are in the form of a square and not a triangle because both the intensity and SAM depend on the azimuthal angle multiplied by four.

In view of Equation (14), near-axis projections of the major axis of polarization ellipse can be approximately deduced from (18) as follows:

$$\begin{aligned} A_x &\approx I_{0,0}\cos(2\varphi) - I_{0,2},\\ A_y &\approx -I_{0,0}\sin(2\varphi),\\ A_z &\approx 0. \end{aligned} \quad (19)$$

From (19), it can be seen that the polarization ellipse major axis vector is predominantly directed downwards in the right upper quadrant, upwards in the left upper quadrant, downwards in the left bottom quadrant, and upwards in the right bottom quadrant. Thus, when making a circle around the central C-point, the ellipse axis vector makes four half-twists, with the polarization singularity index being I = –2.

5. Numerical Modeling

Figure 1 depicts an intensity pattern in the focal plane generated by beam (4), putting $A(\theta) = 1$, a focusing lens with NA = 0.95, and a 532 nm wavelength. The intensity was calculated using Richards–Wolf integrals [3]. From Figure 1, the intensity is seen to form

a triangle with the apex directed downwards, unlike the upwards intensity triangle described in [2]. The polarization states are depicted as ellipses with the major axis denoted by arrows. Red polarization ellipses have a positive z-component of the major axis, whereas blue ellipses have a negative z-component of the major axis, with z denoting the optical axis. An analysis of ellipses located on a circle marked as a white dashed line in Figure 1 shows that the major axis vector of polarization ellipse is directed downwards in the upper right quarter of the circle, upwards in the bottom right quarter, downwards in the bottom left quarter, and upwards in the upper left quarter. Hence, when making a circle around the optical axis, the major axis vector of polarization ellipse can be said to generate a Möbius strip (I = –3/2) with three half-twists at approximate angles of $\varphi = \pi/6$, $3\pi/2$, and $5\pi/6$ and a 'patch' (where two oppositely directed vectors of the polarization ellipse major axis meet) at $\varphi = \pi/2$. We note that the Möbius strip in Figure 1 is rotated by $\pi/2$ relative to the theoretical strip calculated using the approximate relation (14). We also note that, when making a circle around the C-point, the polarization ellipses located close to the center are located on three hyperbolas and make just one half-twist, proving that the polarization singularity of the C-point actually equals I = –1/2. A polarizing Möbius strip on a circle in the form of a white dashed line is shown in Figure 1. It has three half-turns and one stitch at the top, and the index I = −3/2. We also show a polarizing Möbius strip on a circle of smaller radius (gray dotted circle) (Figure 1c). It has one half-turn and one stitch at the bottom, and the index I = −1/2.

Assuming that the Poincaré beam in Equation (1) has topological charges (n, m) = (0, –2), we find that the intensity pattern at the focus forms a square (a yellow-red area in Figure 2) with the central C-point with the polarization singularity index I = –2. Thus, when making a full circle of certain radius around the C-point (white dashed line in Figure 2), the major axis of polarization ellipse will make four half-twists. The index sign is negative because when making a circle anticlockwise, the half-twisted surface also twists anticlockwise. In Figure 2, polarization ellipses on the white circle are directed downwards in the upper right quadrant, upwards in the upper left quadrant, downwards in the bottom left quadrant, and upwards in the bottom right quadrant. Thus, Figure 2 validates the relationship in Equation (19). In a three-dimensional space, the major axis vector of polarization ellipse forms a strip with an even number of half-twists (two half-twisted and two patches). Unlike the Möbius strip (Figure 1), the said strip is two-sided (because of the even number of patches), receiving the name 'twisted ribbon' [4]. We note that, when making a full circle around the C-point inside the intensity square, the polarization ellipses make just two half-twists, proving that the polarization singularity index of the C-point actually equals I = –1.

Interestingly, in Figures 1 and 2, we find separate subwavelength regions containing different-colored polarization ellipses. We recall that red ellipses have a positive tilt relative to the optical axis, while blue ellipses are tilted negatively. The red ellipses denote a positive longitudinal SAM, and the blue ellipses mark negative longitudinal SAM. Because of this, at the focus of both light fields in Equations (4) and (15), a longitudinal optical spin Hall effect occurs, according to which regions with different-signed longitudinal spins are spatially separated [17,18].

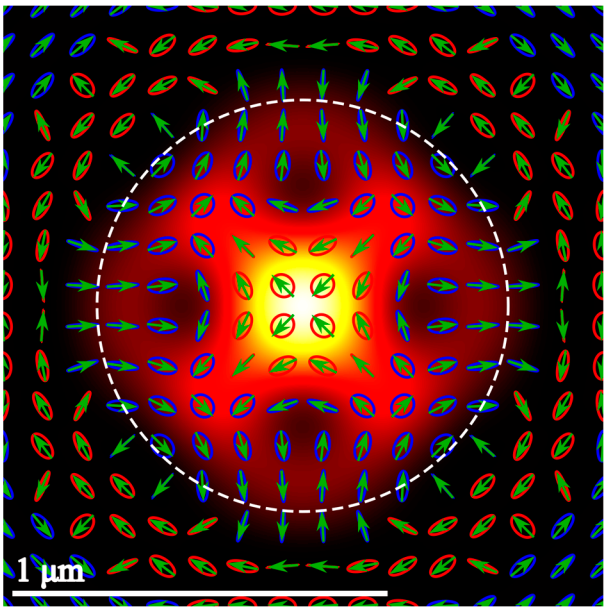

Figure 2. Intensity pattern at the focus for the original field (1) at $n = 0$, $m = -2$ forms a colored (yellow-red) square; green arrows mark the major axis vector of polarization ellipses: red ellipses mark a positive on-axis projection and blue ones mark a negative one. The white horizontal line is 1 um long. The white dashed circle is where a two-sided half-twisted ribbon with four half-twists and index –2 is generated.

6. Discussion of the Results

In this section, we make a detailed comparison of the obtained results with the results of a similar recently published paper [19]. The work [19] does not contain a detailed analytical theory for describing the properties of the intensity, spin and orbital angular momentum, and polarization ellipses in the tight focus. Instead, these characteristics have been only computed numerically. This is the principal difference of our work from the work [19]. The work [19] gives Cartesian components of the intensity distribution (Figure 5 in [19]) in the tight focus of hybrid Poincaré beams from Equation (1) with the vortex topological charges $m = 0$, $n = -1$ and $m = 1$, $n = 0$. They form in the tight focus a triangular intensity distribution, which has in its center a C-point of polarization singularity with the index I = –1/2. In this case, the patterns of polarization ellipses in the focus are the same as that in the initial plane, if $m = 1$, $n = 0$, or is rotated by 180 degrees compared to the initial ellipses pattern if $m = 0$, $n = -1$. The numerical aperture in [19] is equal to NA = 0.95, similar to our work, but the wavelength of light was not given in [19]. In our work, the wavelength is 532 nm, and therefore, the frame size in Figures 1 and 2 slightly exceeds 1 μm. In [19], however, a similar intensity frame has the size (Figure 5 in [19]) of 0.5 μm. This causes doubts since the focal spot in [19] (Figure 5) turns out to be smaller than the wavelength (equal approximately to 0.5:3 = 0.17 μm).

In addition, these two works are different since the patterns with polarization ellipses are significantly different. In work [19], the ellipses pattern in the focus was probably not computed since it is quite the same as that in the initial plane (Figures 2, 3 and 5–7 in [19]). In our work, the ellipses pattern was exactly computed, and it is, therefore, highly diverse (Figure 1). In addition to the polarization ellipses themselves in Figure 1, arrows illustrate the directions of the ellipses' major axes in the same moment of time. Thus, turns of the ellipse arrows indicate half-turns of the Möbius stripe. In addition, ellipse colors in Figure 1 show the tilts of the ellipses along the optical axis (red ellipses) and opposite to the optical axis (blue ellipses). Therefore, Figure 1 practically depicts the 3D distribution of the polarization ellipses, and constructing only the Möbius stripe is already redundant. Analysis of the polarization ellipse pattern in Figure 1 reveals that, with an increasing radius of a circle around the center of the focus, the number of π-turns of the polarization ellipse's

major axis also increases. Along the dashed line in Figure 1, the vector of major polarization axis rotates by the angle 3π, i.e., the polarization singularity index is I = −3/2, and the Möbius stripe makes three half-turns on this radius, and one stitching of oppositely directed vectors of the polarization ellipses' major axes occurs. Furthermore, contrary to work [19], Figure 2 of our work demonstrates a case when the topological charges of the optical vortices of the Poincaré beam (1) are chosen to be equal to $(n, m) = (0, -2)$. In this case, a C-point with an integer polarization singularity index I = –1 is generated in the focus, and, instead of the Möbius stripe, the vectors of polarization ellipses' major axes form a two-sided surface with an even number of half-turns (along a dashed circle in Figure 2).

In the current work, we show theoretically that near the optical axis in the focus plane, polarization indices of the C-points are the same as in the initial plane (Equations (6) and (16.1)). We also show theoretically that the vectors of polarization ellipses in the focus make three half-turns (14) and four half-turns (19) for the two considered initial fields (4) and (15). In [19], polarization ellipses in the focus are just the same as polarization ellipses in the initial plane except for rotation of 180 degrees (Figures 2, 3 and 5–7 in [19]).

In Figures 2, 3 and 5–7 in [19], polarization ellipses show that there are points with circular and elliptic polarization in the initial plane, but it is possible only for definite values B_1, B_2, and θ_0 in Equation (1) in [19], i.e., for definite states on the Poincaré sphere. However, the parameters, for which these polarization ellipses are constructed, are not specified in the paper [19]. In our work, initial states of the Poincaré beams (4) and (15) are chosen with such parameters that the field in the initial plane has inhomogeneous linear polarization, while in the beam center, there is a polarization singularity line at $\varphi = 0$ for the field (4) and V-point of polarization singularity in the center for the field (15). This is another difference of our paper from the work [19], since the choice of inhomogeneous linear polarization in the initial plane allows us to demonstrate arising spin Hall effect in the tight focus. Areas with a different sign of the spin angular momentum are shown in Figures 1 and 2 by red and blue ellipses.

Another difference between our work and work [19] is that the topological charges of the optical vortices were chosen differently. In [19], the topological charges of the Poincaré beam, which generates in the focus a triangular-shaped intensity distribution with a vertex to the top, were chosen as $(n, m) = (0, 1)$. In our work, we chose other topological charges $(n, m) = (0, -1)$. This does not lead to change in the singularity index of the C-point in the center of the focus, I = –1/2, but leads to different polarization states in the initial plane.

Figure 3 illustrates an optical setup that can be used for generating a Poincaré beam (4), for focusing it, and for studying its characteristics with a scanning near-field optical microscope.

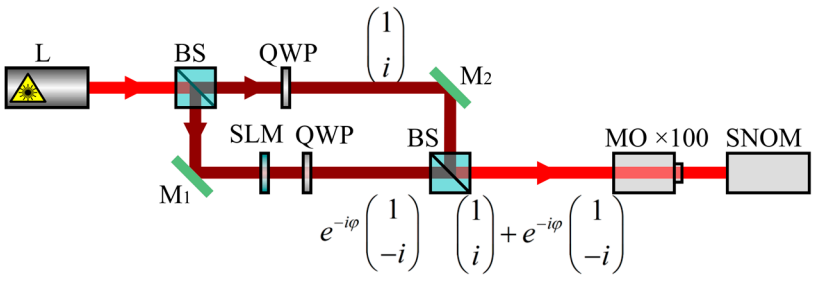

Figure 3. Optical setup for generating and focusing a Poincaré beam (4): L—laser with the wavelength of 532 nm; BS—nonpolarizing beam splitters; QWP—quarter-wave plate; M_1 and M_2—rotatable mirrors; SLM—transmissive liquid-crystal spatial light modulator; MO—microobjective with a 100× zoom (NA = 0.95); and SNOM—scanning near-field optical microscope. Red arrows show the direction of light propagation.

The Mach–Zehnder interferometer setup works as follows. A linearly polarized Gaussian beam comes out of the laser L (wavelength is 532 nm), and then splits into two beams with a beam splitter BS. One beam goes through a quarter-wave plate QWP and acquires right-handed circular polarization, whereas the second beam goes though a modulator SLM and through a rotated QWP and is thus converted to an optical vortex with the topological charge of –1 and with left-handed circular polarization. After the second beam splitter BS, both beams are combined into a single Poincaré beam, which is focused by a microobjective MO to the input of the scanning near-field optical microscope NSOM with a metallic cantilever with a nearly 100 nm hole. Such a microscope allows measuring the intensity distribution near the focus with a space resolution of nearly 30 nm. Shown in Figure 4 are the components of the intensity distribution in the focus plane for initial fields (4) and (15), computed by using the Richards–Wolf formalism [12].

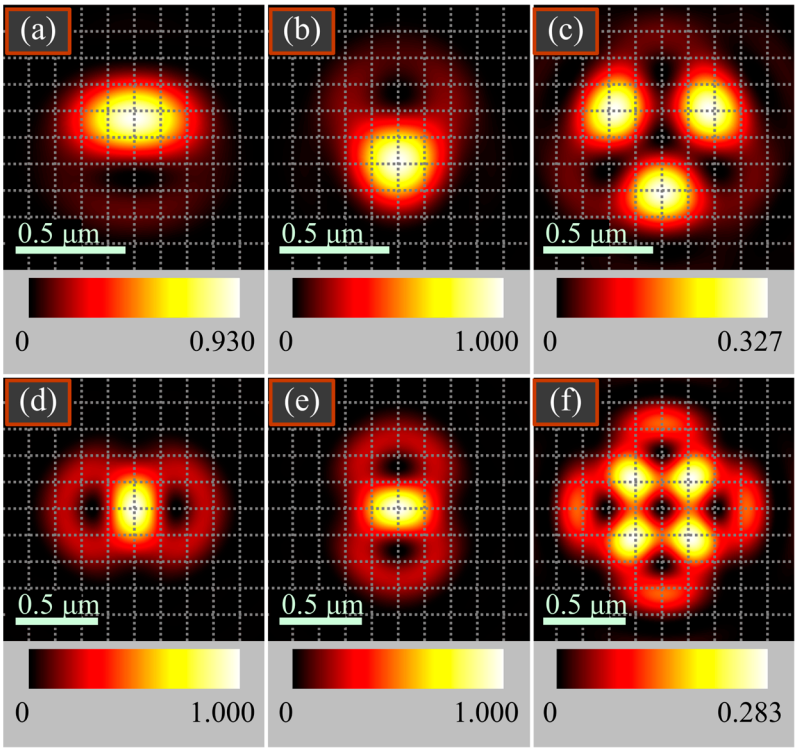

Figure 4. Components of the intensity distribution in the tight focus (NA = 0.95) of the initial beams (4) (**a**–**c**) and (15) (**d**–**f**): I_x (**a**,**d**), I_y (**b**,**e**), and I_z (**c**,**f**). The wavelength is 532 nm, and the initial amplitude of light is constant: $A(\theta) = 1$. The colored bars under the figures describe the intensity values. The frame sizes are 1.2 μm (**a**–**c**) and 1.6 μm (**d**–**f**).

As seen in Figure 4, the initial field (4) generates in the focus the components of the intensity distribution, well described by the formulae (7) and (9). The transverse intensity *Ix* (Figure 4a) has one maximum, shifted to the top along the vertical axis *y*, whereas the intensity *Iy* (Figure 4b) has one maximum, shifted along the vertical axis to the bottom from the optical axis, which is consistent with Equation (9). The longitudinal intensity *Iz* (Figure 4c) has three maxima, according to Equation (7). When these three intensity components are summed up, a triangle is generated with a vertex directed to the bottom (Figure 1). Similarly, the initial field (15) generates in the focus the intensity components, one of which (longitudinal intensity *Iz* in Figure 4f) is described by Equation (18). According to Equation (18), the longitudinal intensity has four maxima in the corners of a square, and the full intensity in the focus of a field (15) has a shape of the square (Figure 2). The colored bars in Figure 4 reveal that the maxima of the transverse intensity are several times higher than the maxima of the longitudinal intensity (since the latter has more maxima).

Figure 5 depicts polarization distributions of the beams (4) and (15) in the initial plane and in the focus plane. According to Figure 5a, in the initial plane of the beam (4), there is a polarization singularity line since at $\varphi = 0$ and at $\varphi = 2\pi$, the linear polarization vectors are opposite. It is also seen that, when passing along some contour around the center of Figure 5a, the vectors rotate by π, i.e., the index of the field (4) is I = –1/2. In center of the focus plane of such a field, a C-point is generated (a point with circular polarization), also with the index I = –1/2 (Figure 5b), but the 'star' structure is rotated by 90 degrees relative to the initial pattern (Figure 5a). We note that there is no such rotation in the polarization pattern in the focus in [19], although it should be present due to the phase singularity of the field (4) with the topological charge $m = -1$. Shown in Figure 5c is distribution of polarization vectors in the initial field (15). It is seen that the vectors are located along hyperbolas and that there is a singularity point (V-point) in the center. When passing around this point, vectors rotate by the angle of 2π, i.e., the index of the V-point equals I = –1. In the focus of the field (15), polarization ellipses are distributed as shown in Figure 5d. In the center of the polarization pattern, a C-point is generated with circular polarization and with the index I = –1. It is clear from Equation (16.1) that, for close values of the integrals $I_{0,0}$~$I_{0,2}$, we can approximately write next expression instead of (16.1):

$$\begin{pmatrix} E_x(r \to 0) \\ E_x(r \to 0) \end{pmatrix} \approx 2I_{0,0}e^{-i\varphi}\begin{pmatrix} \sin\varphi \\ \cos\varphi \end{pmatrix}. \quad (20)$$

It is clear from a comparison of the vectors in parentheses in (15) and (20) that a constant phase equal to $\pi/2$ has been added to the polar angle at the focus. This means that the polarization patterns in the focal plane are rotated by 90 degrees with respect to the polarization vector pattern in the initial plane. Therefore, the linear polarization vectors on the left part of Figure 5a are located vertically, and these linear polarization vectors near the center are located horizontally in Figure 5b (Figure 1a).

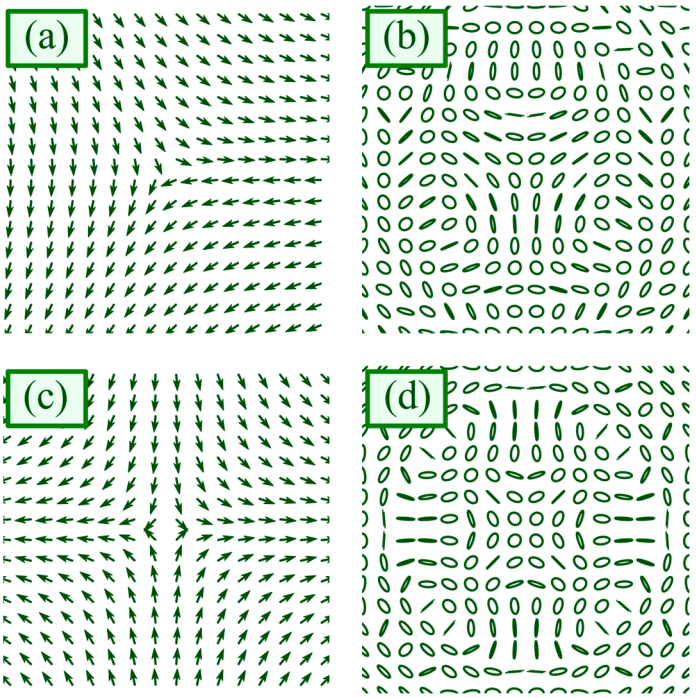

Figure 5. Distributions of linear polarization vectors in the initial plane of the beam (4) (**a**) and of the beam (15) (**c**), as well as distributions of the polarization ellipses in the focus plane of the beam (4) (**b**) and of the beam (15) (**d**). The numerical aperture is 0.95. The frame size is 1 μm (**b**,**d**).

7. Conclusions

Thus, using the Richards–Wolf theory [12], the exact relationships have been deduced for projections of the electric field vector in the focal plane of the generalized Poincaré beam. Analyzing two particular cases of Poincaré beams with topological charges (n, m) = (0, –1) and (n, m) = (0, –2) as an example, it has been shown that, in both cases, at the center of the focal spot, there occurs a circularly polarized C-point surrounded by polarization ellipses that make three (three half-twisted and one patch) and four half-twists (two half-twisted and two patches) when making a full circle of certain radius around the C-point. In a three-dimensional space, when making a full circle, the major axis vectors of polarization ellipse have been shown to generate a one-sided Möbius strip (for an odd number of patches) or a two-sided twisted ribbon (for an even number of patches). It has also been shown that, in both cases, at different regions of the focal plane, the polarization ellipses have a positive or negative tilt with respect to the optical axis. Thus, we infer that ellipses with the longitudinal spins of different signs are separated in the focal spot, demonstrating the presence of a longitudinal optical spin Hall effect.

Application areas of the conducted studies are microstructuring of polarization-sensitive materials [20,21], optical micromanipulations [22,23], and materials micromagnetization [24,25].

Author Contributions: Conceptualization, V.V.K. and A.A.K.; methodology, V.V.K. and A.A.K.; software, A.A.K. and E.S.K.; validation, V.V.K., A.A.K., and E.S.K.; formal analysis, V.V.K. and A.A.K.; investigation, V.V.K., A.A.K., and E.S.K.; resources, V.V.K., A.M.T., and E.S.K.; data curation, V.V.K. and A.A.K.; writing—original draft preparation, V.V.K., A.A.K., and E.S.K.; writing—review and editing, V.V.K., A.A.K., and E.S.K.; visualization, A.A.K. and A.M.T.; supervision, V.V.K.; project administration, A.A.K.; funding acquisition, A.A.K. All authors have read and agreed to the published version of the manuscript.

Funding: The work was partly funded by the Russian Science Foundation under grant # 22-12-00137 (theoretical background) and the NRC 'Kurchatov Institute' under a government project (numerical modeling).

Institutional Review Board Statement: Not applicable.

Informed Consent Statement: Not applicable.

Data Availability Statement: Data is contained within the article.

Conflicts of Interest: The authors declare no conflicts of interest.

References

1. Freund, I. Multitwist optical Möbius strips. *Opt. Lett.* **2010**, *35*, 148–150. https://doi.org/10.1364/OL.35.000148.
2. Bauer, T.; Banzer, P.; Karimi, E.; Orlov, S.; Rubano, A.; Marrucci, L.; Santomato, E.; Boyd, R.W.; Leuchs, G. Observation of optical polarization Möbius strips. *Science* **2015**, *347*, 964–966. https://doi.org/10.1126/science.1260635.
3. Freund, I. Cones, spirals, and Möbius strips, in elliptically polarized light. *Opt. Commun.* **2005**, *249*, 7–22. https://doi.org/10.1016/j.optcom.2004.12.052.
4. Freund, I. Optical Möbius strips, half-twisted ribbons, and the index theorem. *Opt. Lett.* **2011**, *36*, 4506–4508. https://doi.org/10.1364/OL.36.004506.
5. Freund, I. Optical Möbius strips and half-twisted ribbon cloaks. *Opt. Lett.* **2014**, *39*, 727–730. https://doi.org/10.1364/OL.39.000727.
6. Galvez, E.J.; Dutta, I.; Beach, K.; Zeosky, J.J.; Jones, J.A.; Khajavi, B. Multihalf-twist Möbius strips and half-twisted ribbons in the polarization of paraxial light beams. *Sci. Rep.* **2017**, *7*, 13653. https://doi.org/10.1038/s41598-017-13199-1.
7. Bauer, T.; Neugebauer, M.; Leuchs, G.; Banzer, P. Optical polarization Möbius strips and points of purely transverse spin density. *Phys. Rev. Lett.* **2016**, *117*, 013601. https://doi.org/10.1103/PhysRevLett.117.013601.
8. Wan, C.; Zhan, Q. Generation of exotic optical polarization Möbius strips. *Opt. Express* **2019**, *27*, 11516–11524. https://doi.org/10.1364/OE.27.011516.
9. Tekce, K.; Otte, E.; Denz, C. Optical singularities and Möbius strip arrays in tailored non-paraxial light fields. *Opt. Express* **2019**, *27*, 29685–29696. https://doi.org/10.1364/OE.27.029685.
10. Freund, I. Polarization Möbius strips on elliptical paths in threedimensional optical fields. *Opt. Lett.* **2020**, *45*, 3333–3336. https://doi.org/10.1364/OL.392331.

11. Pang, X.; Hu, M.; Liu, W.; Zhao, X. Photonics wheels and polarization Möbius strips in highly-confined trigonometric beams. *IEEE Photonics J*. **2022**, *14*, 6553708. https://doi.org/10.1109/JPHOT.2022.3205640.
12. Richards, B.; Wolf, E. Electromagnetic diffraction in optical systems. II. Structure of the image field in an aplanatic system. *Proc. R. Soc. Lond. A* **1959**, *253*, 358–379. https://doi.org/10.1098/rspa.1959.0200.
13. Beckley, A.M.; Brown, T.G.; Alonso, M.A. Full Poincaré beams. *Opt. Express* **2010**, *18*, 10777–10785. https://doi.org/10.1364/OE.18.010777.
14. Koltyar, V.V.; Nalimov, A.G.; Stafeev, S.S. Exploiting the circular polarization of light to obtain a spiral energy flow at the sub-wavelength focus. *J. Opt. Soc. Am. B* **2019**, *36*, 2850–2855. https://doi.org/10.1364/JOSAB.36.002850.
15. Kovalev, A.A.; Kotlyar, V.V. Spin Hall effect of double-index cylindrical vector beams in a tight focus. *Micromachines* **2023**, *14*, 494. https://doi.org/10.3390/mi14020494.
16. Berry, M.V. Index formulae for singular lines of polarization. *J. Opt. A. Pure Appl. Op.* **2004**, *6*, 675–678. https://doi.org/10.1088/1464-4258/6/7/003.
17. Kotlyar, V.V.; Stafeev, S.S.; Kovalev, A.A.; Zaitsev, V.D. Spin Hall effect before and after the focus of a high-order cylindrical vector beam. *Appl. Sci.* **2022**, *12*, 12218. https://doi.org/10.3390/app122312218.
18. Kotlyar, V.V.; Stafeev, S.S.; Kozlova, E.S.; Butt, M.A. High-order orbital and spin Hall effects at the tight focus of laser beams. *Photonics* **2022**, *9*, 970. https://doi.org/10.3390/photonics9120970.
19. Pal, S.K.; Somers, L.; Singh, R.K.; Senthilkumaran, P.; Arie, A. Focused polarization ellipse field singularities: Interaction of spin-orbit angular momentum and the formation of optical Mobius strips. *Phys. Scr.* **2023**, *98*, 055507. https://doi.org/10.1088/1402-4896/acc89c.
20. Zhang, S.; Liu, W.; Hu, J.; Wang, G.; Wang, Q.; Wang, S.; Wang, S. Polarization sensitive microstructures fabricated on lithium niobate surfaces by using femtosecond laser pulses. *Opt. Express* **2020**, *28*, 7165–7174. https://doi.org/10.1364/OE.387577.
21. Zhai, Y.; Cao, L.; Liu, Y.; Tan, X. A Review of Polarization-Sensitive Materials for Polarization Holography. *Materials* **2020**, *13*, 5562. https://doi.org/10.3390/ma13235562.
22. Kritzinger, A.; Forbes, A.; Forbes, P.B.C. Optical trapping and fluorescence control with vectorial structured light. *Sci Rep*. **2022**, *12*, 17690. https://doi.org/10.1038/s41598-022-21224-1.
23. Yang, Y.; Ren, Y.; Chen, M.; Arita, Y.; Rosales-Guzmán, C. Optical trapping with structured light: A review. *Adv. Photon.* **2021**, *3*, 034001. https://doi.org/10.1117/1.AP.3.3.034001.
24. Lei, X.; Du, L.; Yuan, X.; Zayats, A.V. Optical spin–orbit coupling in the presence of magnetization: Photonic skyrmion interaction with magnetic domains. *Nanophotonics* **2021**, *10*, 3667–3675. https://doi.org/10.1515/nanoph-2021-0201.
25. Dąbrowski, M.; Guo, S.; Strungaru, M.; Keatley, P.S.; Santos, E.J.; Hicken, R.J. All-optical control of spin in a 2D van der Waals magnet. *Nat. Commun.* **2022**, *13*, 5976. https://doi.org/10.1038/s41467-022-33343-4.